Check for updates

Preparation of PVA/cellulose composite hydrogel electrolytes based on zinc chloride-dissolved cellulose for flexible solid-state capacitors†

Ru Zhang,[a] Chengfeng Wu,*[a] Xuyan Liao,[a] Axi Luo,[a] Yidan Jing,*[a] Ningya Yu,[a] Shengpei Su,[a] Xiaomin Zhang, [ID]*[a] Jin Zhu[b] and Guobo Deng[a]

The PVA-based hydrogel electrolyte, characterized by its high ionic conductivity and degradability, holds significant promise for applications in flexible supercapacitors. However, pure PVA hydrogel electrolytes have suffered from deficiencies in flexibility, self-healing properties, and anti-freezing performance. In this study, a novel approach was employed by *in situ* blending polyvinyl alcohol (PVA) with zinc chloride (ZnCl$_2$) dissolved cellulose. When the mass ratio of PVA to cellulose was 2 : 1, the resulting PVA/cellulose composite hydrogel electrolyte exhibited a commendable tensile strength (198 kPa) and remarkably high elongation at break (2415%); the assembled zinc/carbon asymmetric supercapacitor demonstrated an area-specific capacitance of 636 mF cm^{-2} (2 mA cm^{-2}). Moreover, at −30 °C, the capacitance retention exceeded 94%, indicating excellent anti-freezing properties. Subsequent electrical performance tests on the self-healed hydrogel electrolyte capacitors yielded a capacitance retention rate exceeding 94%, demonstrating outstanding self-healing properties. This novel class of hydrogel electrolytes provides a viable research perspective for addressing the aforementioned issues. Additionally, this study also involved straightforward treatment of used hydrogels, allowing for the recovery of high-value zinc salts such as zinc carbonate and zinc chloride, with a recycling efficiency as high as 55%. The entirety of the experiment exhibited an environmentally friendly and sustainable engineering process.

Introduction

In recent years, hydrogels have gained prominence as flexible solid electrolytes for applications in flexible supercapacitors, owing to their excellent flexibility,[1,2] high water content conducive to salt incorporation,[3] ease of processing, and resistance to liquid leakage.[4] Common substrates include polyacrylamide (PAM),[5] polyacrylic acid (PAA),[6] and polyvinyl alcohol (PVA).[7–11] Among these, PVA-based hydrogel electrolytes are extensively utilized on account of their non-toxicity, high ionic conductivity, and degradability, aligning with the sustainable development

requirements of green chemistry.[12] However, pure PVA hydrogel electrolytes have suffered from drawbacks such as poor flexibility, limited self-healing capability, and reduced capacitance performance at low temperatures, thus impeding their large-scale application.[13,14]

The current primary research direction mainly focuses on incorporating inorganic fillers within PVA-based hydrogels to obtain hydrogel electrolytes with desirable mechanical and electrical properties. For instance, Xu *et al.*[15] introduced graphene into a PVA–PET network, resulting in a dual-network PET–PVA hydrogel capable of delivering a specific capacitance of 281.2 F g^{-1} at room temperature (0.1 A g^{-1}). Subsequently, Tian *et al.*[16] introduced MXenes into the PVA network, synthesizing a novel cross-linked hydrogel electrolyte that further enhanced the specific capacitance of PVA hydrogel electrolytes (130.8 mF cm^{-2}, 1 mA cm^{-2}). Nevertheless, the anti-freezing performance of such hydrogel electrolytes remains limited. To improve the anti-freezing properties, it is common to employ methods involving the addition of organic antifreeze agents.

For example, Zhu *et al.*[17] introduced glycerol into PVA hydrogel electrolytes, resulting in PGS hydrogel electrolytes with a capacitance retention of 56.3% at −20 °C. Additionally, Liu *et al.*[18] introduced 1-ethyl-3-methylimidazolium acetate (EMImAc) ionic

[a] *Key Laboratory of Chemical Biology and Traditional Chinese Medicine Research (Ministry of 'Education of China), The Key Lab for Fine Processing of Resources and Advanced Materials of Hunan Province, National and Local Joint Engineering Lab for New Petro-chemical Materials and Fine Utilization of Resources, Hunan Normal University, Changsha 410081, People's Republic of China.*
E-mail: 202120122411@hunnu.edu.cn, jingyd@hunnu.edu.cn, zhangxm@hunnu.edu.cn

[b] *Key Laboratory of Bio-based Polymeric Materials, Ningbo Institute of Material Technology and Engineering, Chinese Academy of Sciences, Ningbo 315201, People's Republic of China*

† Electronic supplementary information (ESI) available. See DOI: https://doi.org/10.1039/d3tc03988a

This journal is © The Royal Society of Chemistry 2024

J. Mater. Chem. C, 2024, **12**, 2063–2072 | **2063**

liquid into PVA hydrogel electrolytes, further enhancing their anti-freezing properties. The resultant hydrogel electrolytes maintained a degree of flexibility and conductivity even at $-50\ °C$. However, it is worth noting that such methods not only entail complex preparation processes but also require further evaluation of the environmental impact of the introduced organic solvents and ionic liquids.[19–22]

One of the primary approaches to address the aforementioned issues is the incorporation of renewable natural high-molecular-weight materials into PVA-based hydrogels to prepare high-performance composite hydrogel electrolytes. Examples of such materials include chitosan,[23] sodium alginate,[24] and cellulose.[25–28] Among them, cellulose is the most abundant natural polymer globally and finds its widespread application in modified PVA hydrogels.[29] Currently, most studies utilized nanocellulose and cellulose derivatives in conjunction with PVA to fabricate composite hydrogel electrolytes, thereby enhancing various properties of PVA hydrogel electrolytes.[9,30–32]

For instance, Zhao et al.[33] prepared a PVA-cellulose hydrogel that can be employed in flexible solid-state zinc–air batteries by combining PVA with bacterial cellulose (BC) ultrafine fibers, exhibiting a high ionic conductivity of 80.8 mS cm^{-1}. Subsequently, Hu et al.[7] utilized cellulose nanofibers (CNFs) and PVA to fabricate PVA-CNF composite hydrogels, resulting in electrolytes with an exceptionally high fracture elongation of 242% and an ionic conductivity of 0.32 S m^{-1}. This further augmented their mechanical strength. However, it is worth noting that such methods cause relatively high energy consumption for nanocellulose preparation. Zhu et al.[12] introduced carboxymethyl cellulose (CMC) into PVA to prepare PVA/CMC composite hydrogel electrolytes. Additionally, with the inclusion of zinc trifluoromethanesulfonate ($Zn(CF_3SO_3)_2$), the obtained hydrogel electrolyte demonstrated the ability to maintain a high energy density (60.7 W h kg^{-1}) at low temperatures ($-20\ °C$). Nevertheless, the addition of cellulose derivatives not only incurs higher energy consumption during synthesis but also results in relatively lower toughness of the composite hydrogel. Thus, adding nanocellulose or cellulose derivatives to prepare PVA/cellulose composite hydrogels poses challenges in terms of energy consumption, process complexity, and limited enhancement effects.[34] In our previous work, cellulose dissolved in H_3PO_4 was directly combined with PVA to fabricate PVA/cellulose composite hydrogel electrolytes, which not only exhibited extremely high mechanical properties (200 kPa, 1173%) but also demonstrated exceptional capacitive performance (217 mF cm^{-2}) when used in supercapacitors. However, the phosphoric acid dissolution system poses challenges related to solvent recovery and has a certain level of toxicity.

This study proposes to utilize a zinc chloride solution for cellulose dissolution, directly employed in the fabrication of PVA/cellulose composite hydrogel electrolytes, offering advantages of a simplified process and lower energy consumption.[35] Zinc chloride serves not only as an electrolyte solution but also as an antifreeze agent,[36] imparting excellent freeze resistance to the hydrogel electrolyte.[37–40] Furthermore, by leveraging the nontoxic and easily recoverable nature of zinc chloride, a straightforward method is designed for the recovery and recycling of zinc

salts, addressing the aforementioned issues. In this process, a high-concentration zinc chloride cellulose solution is mixed with a PVA aqueous solution. Through the chemical cross-linking of borax and the ion cross-linking of Ca^{2+}, a multifunctional PVA/cellulose composite hydrogel electrolyte was prepared, exhibiting high specific capacitance, flexibility, freeze resistance, and self-healing properties. It is anticipated that this electrolyte holds promising prospects in the field of flexible supercapacitors. Additionally, the fabricated PVA/cellulose composite hydrogel electrolyte poses minimal environmental harm and allows for the facile recycling of zinc salts, offering a new approach for the design of economically viable and environmentally friendly multifunctional flexible solid-state electrolytes.

Results and discussion

A composite hydrogel is obtained by mixing PVA with cellulose dissolved in a high-concentration zinc chloride solution, as shown in Fig. 1. The abundance of hydrogen bonds formed between PVA chains and cellulose fibers significantly enhances the mechanical properties of the composite hydrogel material. This preparation strategy offers advantages such as the simplicity of operation and minimal environmental impact. Additionally, it maximizes the various uses of zinc chloride, ensuring high specific capacitance of the supercapacitor, enhancing the freeze resistance of the hydrogel electrolyte through strong hydration, and providing excellent thermoplastic and self-healing abilities. It is worth noting that discarded gels can undergo a simple process for solvent recycling. It is anticipated that this approach holds great potential for advancement in the field of flexible supercapacitors. The test results and analysis for the novel PVA-cellulose hydrogel electrolyte are presented below:

To investigate the influence of the mass ratio of PVA to cellulose on the mechanical properties of the hydrogel electrolyte, stress–strain tests were conducted on PVA/cellulose hydrogel electrolytes with different mass ratios (Fig. 2a and a′). The mechanical properties of the pure zinc chloride cellulose hydrogel (ZCE hydrogel) and PVA/cellulose composite hydrogel (1P-CE hydrogel) (detailed formulation in Table S1, ESI†) were so poor that cannot withstand the pressure of the universal
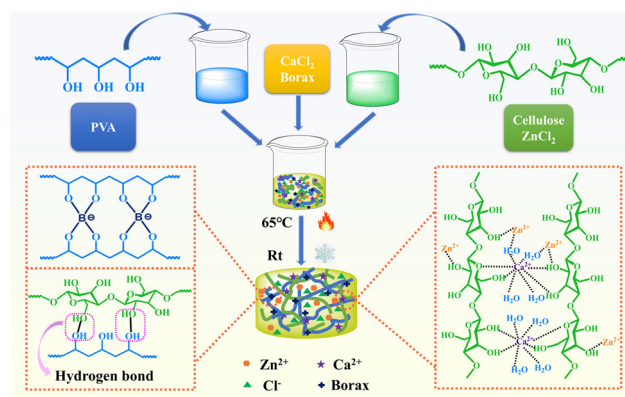

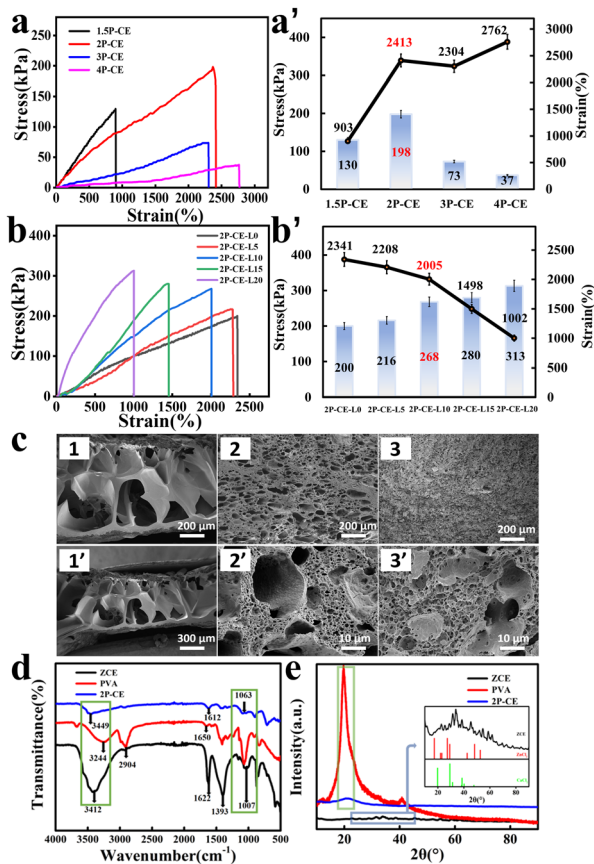Fig. 1 Schematic diagram of PVA-cellulose hydrogel preparation.

2064 | J. Mater. Chem. C, 2024, **12**, 2063–2072

This journal is © The Royal Society of Chemistry 2024

Fig. 2 (a) and (a′) Stress−strain curves of the PVA/cellulose composite hydrogel. (b) and (b′) Stress−strain curves of the PVA/cellulose/LiCl composite hydrogel. (c) SEM images of the ZCE (c1) and (c1′), 2P-CE (c2) and (c2′), and 2P-CE-L10 (c3) and (c3′) hydrogels. (d) FTIR spectra. (e) XRD patterns.

testing machine (Fig. S1, ESI†). Therefore, the testing was initiated using the 1.5P-CE hydrogel (hydrogel formulation of PVA: cellulose 1.5 : 1) to record the test results. The results indicate that as the PVA content increases, the tensile strength of the PVA/cellulose hydrogel electrolyte initially increases and then declines. When the PVA/cellulose ratio is 2 : 1, the tensile strength of the 2P-CE hydrogel electrolyte is the highest, reaching 198 kPa, with a fracture elongation rate of 2413%. Meanwhile, the 2P-CE hydrogel electrolyte has a Young's modulus of 7.5×10^{-3} MPa (Fig. S2a, ESI†), which is sufficient for its application in flexible super-capacitors. This can be attributed to the interaction between PVA and cellulose, which densifies and stabilizes the internal structure of the gel, thereby enhancing its tensile strength. However, the excessive PVA content leads to a reduction in inter-chain cross-linking density of cellulose, disrupting the internal structure of the hydrogel and subsequently lowering the tensile strength. There-fore, although increasing the PVA content in the composite hydrogel electrolyte leads to a continuous increase in fracture elongation and a decrease in Young's modulus, suggesting improved flexibility, the tensile strength becomes too low to meet the requirements of flexible supercapacitors. Hence, the 2P-CE hydrogel electrolyte is chosen for further exploration.

Subsequently, stress–strain tests were conducted on the PVA/cellulose/LiCl hydrogel electrolyte immersed in LiCl/CaCl$_2$ solution (Fig. 2b and b′). The results indicate that as the concentration of LiCl solution increases, the tensile strength of the PVA/cellulose/LiCl hydrogel electrolyte continuously increases, while the fracture elongation shows varying degrees of decrease. At the same time, the Young's modulus of the PVA/cellulose/LiCl hydrogel electrolyte keeps increasing, demon-strating that as the concentration of LiCl increases, the flex-ibility of the hydrogel electrolyte decreases, and the tensile strength increases.

Among them, the composite hydrogel electrolyte immersed in 10 wt% LiCl (2P-CE-L10 hydrogel) (Table S2, ESI†) not only has a tensile strength of 268 kPa and a fracture elongation of 2005% but also possesses a Young's modulus of 13.5×10^{-3} MPa (Fig. S2b, ESI†). These results are because the salting-out effect strengthens with increasing salt concentration, and the addition of hydrophilic salts causes the hydrogel to dehydrate, enhancing the polymer chain friction and effectively improving the mechanical strength, resulting in the hydrogel becoming harder.[41] Additionally, the presence of CaCl$_2$ in the solution increases the cross-linking density of the hydrogel electrolyte, thereby increasing its tensile strength, consistent with the microstructure of the hydrogel. This result is consistent with the microstructure of the hydrogel.

As shown in the SEM images of various hydrogels (Fig. 2c), the internal structure of the ZCE hydrogel exhibits large and uneven pore sizes (Fig. 2c1-1′), while the 2P-CE (Fig. 2c2-2′) and 2P-CE-L10 (Fig. 2c3-3′) hydrogel electrolytes have smaller and more uniformly distributed pore structures. Compared to the loose structure inside the ZCE hydrogel, the internal structures of the 2P-CE and 2P-CE-L10 hydrogel electrolytes are denser and more uniform. This is advantageous for energy dissipation when subjected to changes in stress, resulting in higher mechanical performance. After soaking in the electrolyte, the pore structure of the 2P-CE-L10 hydrogel electrolyte is denser compared to that of the 2P-CE hydrogel electrolyte. This can be attributed to the increased cross-linking of cellulose due to the entry of a large amount of Ca^{2+}, resulting in a more uniform and dense internal structure. This structure also facilitates ion transport, contributing to the enhancement of the hydrogel electrolyte's electrochemical performance.

Subsequently, FTIR and XRD were employed to characterize the structural composition of the PVA/cellulose composite hydrogel electrolyte. The FTIR spectra are shown in Fig. 2d. Characteristic peaks of the ZCE appear at 3412 cm^{-1}, representing the stretching vibration peak of -OH. Peaks at 1622 cm^{-1} and 1393 cm^{-1} correspond to the bending vibrations of adsorbed water's O–H and the shearing vibration of -CH$_2$ groups, respectively. The peak at 1007 cm^{-1} corresponds to the stretching vibration of ether bonds. PVA exhibits characteristic peaks at 3244 cm^{-1} for the –OH stretching vibration, 2904 cm^{-1} for the C–H stretching vibration, 1650 cm^{-1} for the C=O stretching vibration of ester groups, and 1063 cm^{-1} for the C–O stretching vibration. In the 2P-CE, the –OH characteristic peak is around 3449 cm^{-1}, shifted to lower wavenumbers, indicating interactions between the cellulose and

This journal is © The Royal Society of Chemistry 2024

J. Mater. Chem. C, 2024, **12**, 2063–2072 | **2065**

PVA chains, implying the formation of intermolecular hydrogen bonds between cellulose and PVA. Furthermore, the hydroxyl peak of PVA at 1063 cm^{-1} is almost absent in the 2P-CE, confirming the formation of hydrogen bonds between the –OH groups of PVA and cellulose.[7]

The XRD spectra of ZCE, PVA, and 2P-CE hydrogel electrolytes (Fig. 2e) reveal that the characteristic diffraction peak of the 2P-CE hydrogel appears at $2\theta = 20.6°$, which is approximately in line with that of the PVA hydrogel ($2\theta = 19.5°$). However, the intensity of the diffraction peak of the pure PVA hydrogel is significantly higher than that of the 2P-CE hydrogel, indicating that the introduction of cellulose reduces the crystallinity of the PVA hydrogel. By comparing the diffraction patterns of the zinc chloride cellulose hydrogel (ZCE) with those of zinc chloride and calcium chloride, it can be observed that zinc chloride exhibits strong diffraction peaks at $2\theta = 17°, 27°, 29°, 48°,$ and $52°$, while calcium chloride mainly displays diffraction peaks at $2\theta = 19.8°,$ $20°,$ and $38.6°$. In contrast, the primary diffraction peaks of the ZCE are relatively right shifted compared to those of zinc chloride and calcium chloride ($2\theta = 22.7°, 25.6°, 31.6°, 33.7°, 38.6°, 45.5°,$ $54.5°, 58.8°,$ and $61.9°$). This phenomenon arises from the interaction between cellulose and zinc chloride, as well as calcium chloride in the ZCE, leading to alterations in its diffraction peaks. In summary, we have successfully fabricated a hydrogel electrolyte with a dual cross-linked network composed of cellulose and PVA.

Based on the excellent mechanical properties of the PVA-cellulose hydrogel electrolyte, we further investigated its electrochemical performance. Using the PVA/cellulose hydrogel as the electrolyte and activated carbon as the symmetric electrode, a supercapacitor was assembled for electrochemical performance testing. The CV and GCD curves are shown in Fig. 3a and b, respectively. All composite hydrogel electrolytes exhibit good symmetry in CV curves, and their GCD curves approximate symmetric isosceles triangles. This indicates good Coulombic efficiency and minimal capacitance loss during charge and discharge, demonstrating favorable electrochemical performance. The specific area capacitance of the 2P-CE hydrogel electrolyte at a current density of 2 mA cm^{-2} is 130 mF cm^{-2}. Submerging the 2P-CE hydrogel in a high-concentration electrolyte salt solution for 24 hours to reach equilibrium significantly enhances the specific capacitance of the hydrogel electrolyte. Specifically, the P-CE-L10 hydrogel electrolyte (immersed in a 10 wt% LiCl electrolyte solution) exhibits the highest specific area capacitance of 218 mF cm^{-2} and a maximum energy density of 1.94×10^{-2} mW h cm^{-2} at a power density of 0.8 mW cm^{-2}. The electrochemical impedance spectra (EIS) of the composite hydrogel electrolytes in Fig. 3d reveal that the bulk resistance of the 2P-CE hydrogel electrolyte reaches a maximum of 2.27 Ω, whereas the P-CE-L10 hydrogel electrolyte (immersed in a 10 wt% LiCl electrolyte solution) has the lowest bulk resistance of 1.23 Ω, resulting in an ion conductivity of 8.13×10^{-2} S cm^{-1}. Fig. 3e and f display the CV and GCD curves of the optimal-performing 2P-CE-L10 hydrogel electrolyte at different scan rates and current densities. At current densities of 2, 3, 5, 8, and 10 mA cm^{-2}, the specific area capacitances of the super-capacitor are 218, 205, 192, 170, and 170 mF cm^{-2}, respectively
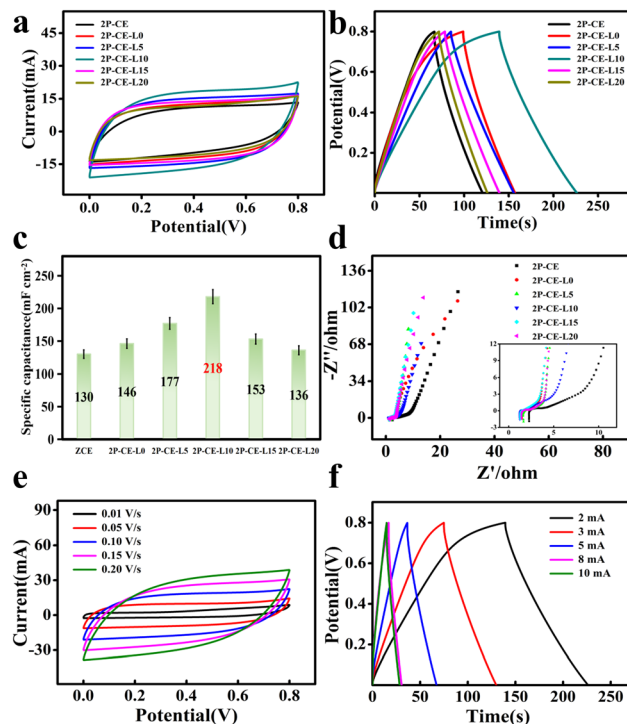

Fig. 3 (a) CV curves of activated carbon symmetric capacitors assembled with different hydrogel electrolytes. (b) GCD curves, (c) capacitance comparison chart, (d) EIS spectrum, and (e) CV curves of the 2P-CE-L10 hydrogel electrolyte. (f) GCD curves.

(Fig. 3c). All composite hydrogel electrolytes exhibit good symmetry in CV curves, and their GCD curves approximate symmetric isosceles triangles, indicating favourable Coulombic efficiency and minimal capacitance loss during charge and discharge, showcasing excellent electrochemical performance. The ion conductivity of the P-CE-L10 hydrogel electrolyte is 8.13×10^{-2} S cm^{-1}, and it achieves a maximum energy density of 1.94×10^{-2} mW h cm^{-2} at a power density of 0.8 mW cm^{-2}.

Similarly, using the PVA/cellulose hydrogel as the electrolyte, activated carbon coated on foam nickel as the carbon electrode, and polished and cleaned zinc sheets as the zinc electrode, an asymmetric zinc/carbon supercapacitor with a sandwich structure was assembled. The electrochemical performance test results are shown in Fig. 4a–c. At a current density of 2 mA cm^{-2}, the specific area capacitance of the 2P-CE hydrogel electrolyte is 445 mF cm^{-2}, while that of the 2P-CE-L10 hydrogel electrolyte is 636 mF cm^{-2}. Fig. 4e and f show the CV and GCD curves of the 2P-CE-L10 hydrogel electrolyte when assembled in a zinc/carbon asymmetric supercapacitor. From the EIS spectrum in Fig. 4d, it can be calculated that the ion conductivity of the 2P-CE-L10 hydrogel electrolyte is 6.58×10^{-2} S cm^{-1}, and it achieves a maximum energy density of 5.65×10^{-2} mW h cm^{-2} at a power density of 0.8 mW cm^{-2}. In summary, the PVA/cellulose hydrogel electrolyte we prepared exhibits outstanding electrochemical performance in both carbon–carbon symmetric capacitors and zinc-carbon asymmetric capacitors, providing a solid foundation for its application in flexible electronic devices.

2066 | J. Mater. Chem. C, 2024, 12, 2063–2072

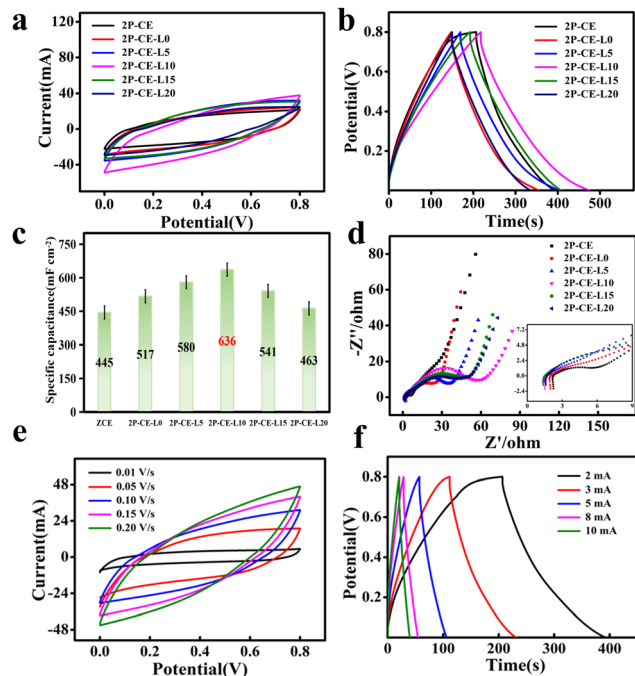This journal is © The Royal Society of Chemistry 2024

Fig. 4 (a) CV curves of zinc/carbon asymmetric capacitors assembled with different hydrogel electrolytes. (b) GCD curves, (c) capacitance comparison chart, (d) EIS spectrum, and (e) CV curves of the 2P-CE-L10 hydrogel electrolyte. (f) GCD curves.
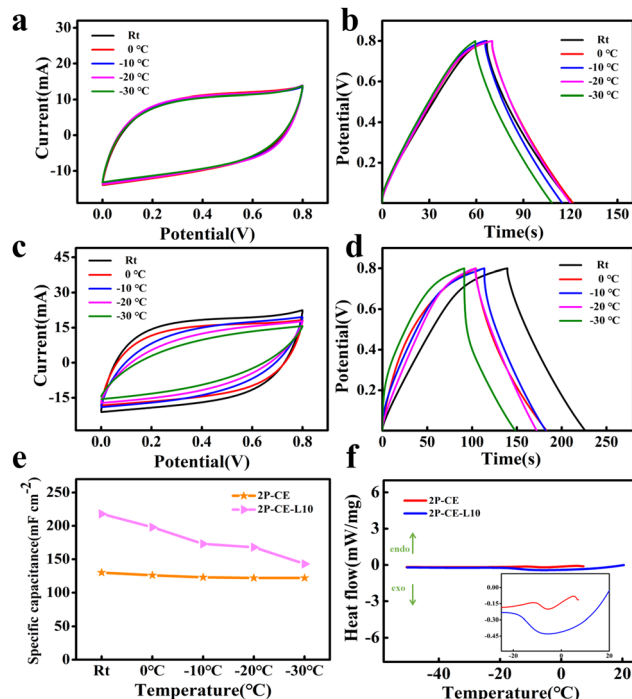

Fig. 5 (a) CV curves of the 2P-CE hydrogel at different temperatures. (b) GCD curves and (c) CV curves of the 2P-CE-L10 hydrogel at different temperatures. (d) GCD curves. (e) Specific capacitance chart. (f) DSC curves.

Next, the activated carbon symmetric supercapacitor assembled with the 2P-CE and 2P-CE-L10 hydrogel electrolytes was subjected to charge–discharge cycling tests at a current density of 3 mA cm^{-2}. The results in Fig. S3a (ESI†) show that after 1200 cycles of charge and discharge, the specific capacity retention of the 2P-CE hydrogel is 48%, and that of the 2P-CE-L10 hydrogel electrolyte is 49%. Then, the zinc/carbon asymmetric supercapacitor assembled the with 2P-CE and 2P-CE-L10 hydrogel electrolytes was subjected to charge–discharge cycling tests at a current density of 5 mA cm^{-2}. The results in Fig. S3b (ESI†) show that after 2500 cycles of charge and discharge, the specific capacity retention of the 2P-CE hydrogel is 49%, and that of the 2P-CE-L10 hydrogel electrolyte is 54%. The experimental results indicate that compared to the activated carbon symmetric supercapacitor, the assembled zinc/carbon asymmetric supercapacitor exhibits higher capacitance performance and cycle life. This is attributed to the fact that in the activated carbon symmetric supercapacitor, despite showing excellent double-layer capacitance behaviours, the deposition of some zinc ions is unavoidable. This is because the attraction effect of zinc ions by the negative charge on the electrode is greater than the diffusion effect of the double-layer potential drop. After long cycles, due to the deposition of zinc ions and the decrease in the ion concentration inside the hydrogel electrolyte, the capacitance retention is poor. Conversely, the zinc/carbon asymmetric supercapacitor achieves a relative balance in the deposition and stripping of zinc ions at the zinc electrode interface, significantly improving the capacitance retention after long cycles.[42] This insight provides inspiration for the development of flexible zinc ion capacitors.[43]

To investigate the influence of high-concentration zinc chloride solution on the antifreeze performance of PVA/cellulose hydrogel electrolytes, electrochemical performance tests were conducted on capacitors assembled with 2P-CE hydrogel electrolytes at different temperatures. The results, as shown in Fig. 5a and b, reveal that the cyclic voltammetry (CV) curves of the supercapacitors at different temperatures remained largely unchanged, with a capacity retention rate of over 94% at −30 °C. Simultaneously, the hydrogel maintained high flexibility at low temperatures (Fig. S4, ESI†). This suggests that the high-concentration zinc chloride solution plays a crucial role in enhancing the antifreeze performance of the hydrogel electrolyte. The water molecules in the hydrogel are tightly bound due to the strong hydrating effect of zinc chloride, inhibiting the formation of ice crystals at low temperatures. This, in turn, has no impact on the transport of ions in the hydrogel electrolyte, endowing the device with outstanding antifreeze performance.[44]

Similarly, the capacitors assembled with 2P-CE-L10 hydrogel electrolytes underwent the same tests, and the results are shown in Fig. 5c and d. It can be observed that after immersion in the aqueous solution, the antifreeze performance of the 2P-CE-L10 hydrogel electrolyte slightly declined. This may be attributed to the reduction in the zinc chloride concentration after immersion in the electrolyte solution, resulting in a decrease in the hydrating effect on free water, thus allowing ice crystal formation and a slight reduction in antifreeze performance. However, the assembled supercapacitor still exhibited high capacitance performance, surpassing that of the capacitors assembled with 2P-CE

This journal is © The Royal Society of Chemistry 2024

J. Mater. Chem. C, 2024, 12, 2063–2072 | 2067

hydrogel electrolytes. Fig. 5e depicts the trend of specific area capacitance of supercapacitors assembled with the 2P-CE and 2P-CE-L10 hydrogel electrolytes with varying temperatures. Fig. 5f displays the differential scanning calorimetry (DSC) curves of 2P-CE and 2P-CE-L10 hydrogel electrolytes. It is evident from the figure that at low temperatures, both hydrogel electrolytes exhibit minimal crystalline peaks of water, approximating a straight line. Only weak peaks of free water crystallization are observed near 0 °C, with those of the 2P-CE being weaker and narrower compared to those of 2P-CE-L10 hydrogel electrolytes.

These results collectively demonstrate that the prepared supercapacitors maintain high electrochemical performance and flexibility even at low temperatures. This affirms the advantages of PVA/cellulose hydrogel electrolytes, which possess excellent antifreeze properties, environmental stability, and a broad range of practical application temperatures.

In addition to demanding high specific capacitance, the self-healing ability of hydrogel electrolytes is one of the most crucial properties for flexible capacitors. Here, an investigation into the self-healing capability of PVA-cellulose hydrogel electrolytes is presented. Firstly, the thermoplasticity of the PVA/cellulose hydrogel was demonstrated (Fig. S5, ESI†). The PVA/cellulose hydrogel electrolyte, already solidified in a plastic bottle (Fig. S5a, ESI†), was heated at 80 °C. Within half an hour, it transformed back into a flowable solution state (Fig. S5b, ESI†). Then, the mixed PVA/cellulose solution was laid flat and left to stand (Fig. S5c, ESI†). Once the solution temperature cooled to room temperature, it solidified back into a hydrogel electrolyte (Fig. S5d, ESI†). These experimental results indicate that the PVA/cellulose hydrogel exhibits excellent thermoplasticity, and further verifies its self-healing capability (Fig. S5e, ESI†).

Heating promotes the free movement and mutual penetration of PVA chains and cellulose chains in the entangled region of the PVA/cellulose hydrogel electrolyte. The original cross-linking structure and hydrogen bonding network at the fracture site was disruption; after cooling, Ca^{2+} and Zn-cellulose portions at the fracture site can form a new ion-crosslinked network through synergistic interactions. Simultaneously, a large number of hydrogen bonds are formed between PVA and cellulose chains, constituting a hydrogen bond network. The combined action of these processes ultimately achieves self-healing of the hydrogel electrolyte.[37] Subsequently, tensile performance tests were conducted on hydrogels with different self-healing times using a universal testing machine. The experimental results indicate that at 80 °C, with the increase in self-healing time, the mechanical properties of the hydrogel electrolyte gradually strengthened after self-healing (Fig. 6a and b). When the self-healing time reached 30 minutes, its tensile strength already exceeded the initial strength (198 kPa). This is because at high temperatures, partial evaporation of water and thermal motion of cellulose and PVA chains shortened the distance between chains, leading to a significant increase in tensile strength. When the heating time was too long, reaching 2 hours, water loss became more severe, disrupting the internal structure of the gel, resulting in a slight decrease in the tensile strength.

Therefore, with a self-healing time of 1 hour, the PVA/cellulose hydrogel electrolyte exhibited the best tensile strength
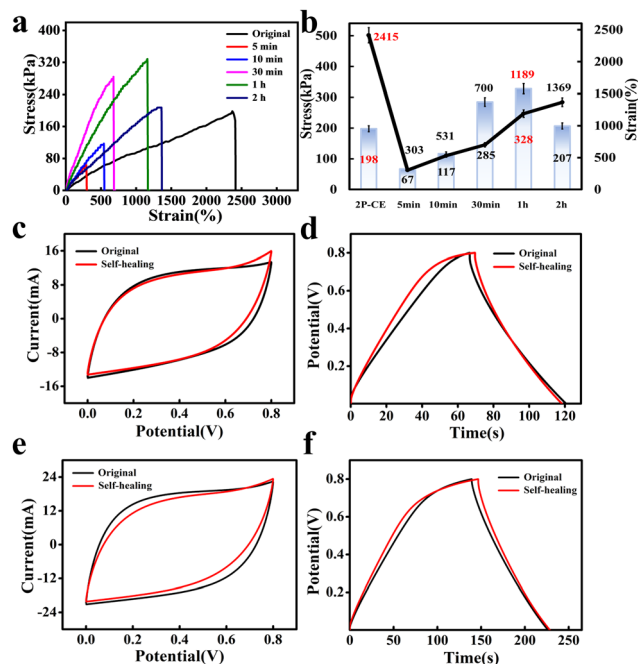

Fig. 6 (a) and (b) Mechanical properties of the self-healed 2P-CE hydrogel. (c) and (d) Electrical properties of the 2P-CE hydrogel before and after self-healing. (e) and (f) Electrical properties of the 2P-CE-L10 hydrogel before and after self-healing.

and elongation at break, indicating the most effective self-healing performance. Fig. 6c, d and e, f respectively present the electrochemical performance test results after self-healing of 2P-CE and 2P-CE-L10 hydrogel electrolytes. After self-healing, the assembled supercapacitor of the 2P-CE hydrogel electrolyte exhibited an area-specific capacitance of 123 mF cm^{-2} and a capacitance retention rate of 95% at a current density of 2 mA cm^{-2}. For the 2P-CE-L10 hydrogel electrolyte, after self-healing, the device demonstrated an area-specific capacitance of 204 mF cm^{-2} and a capacitance retention rate of 94% at a current density of 2 mA cm^{-2}. The high capacitance retention rate demonstrates the excellent self-healing performance of PVA/cellulose hydrogel electrolytes, which holds significant implications for extending the device's operational lifespan.

In addition, considering the effect of multiple bending cycles on the performance of the capacitor, the mechanical properties of 2P-CE and 2P-CE-L10 hydrogel electrolytes were investigated after 500 bending cycles, along with their electrochemical performance when assembled into symmetric capacitors. As shown in Fig. 7a and b, there is no significant change in the tensile strength, fracture elongation, and Young's modulus of the gel after multiple bending cycles; similarly, as depicted in Fig. 7c–f, the CV and GCD curves show no noticeable variation after repeated bending cycles, and the capacitance retention remains above 97%. These observations confirm that the prepared composite hydrogel electrolyte exhibits excellent flexibility, suggesting promising prospects for its application in flexible supercapacitors.

To explore the application prospects and the environmental and economic value of the PVA/cellulose hydrogel, a symmetric supercapacitor assembled with the 2P-CE-L10 hydrogel electrolyte
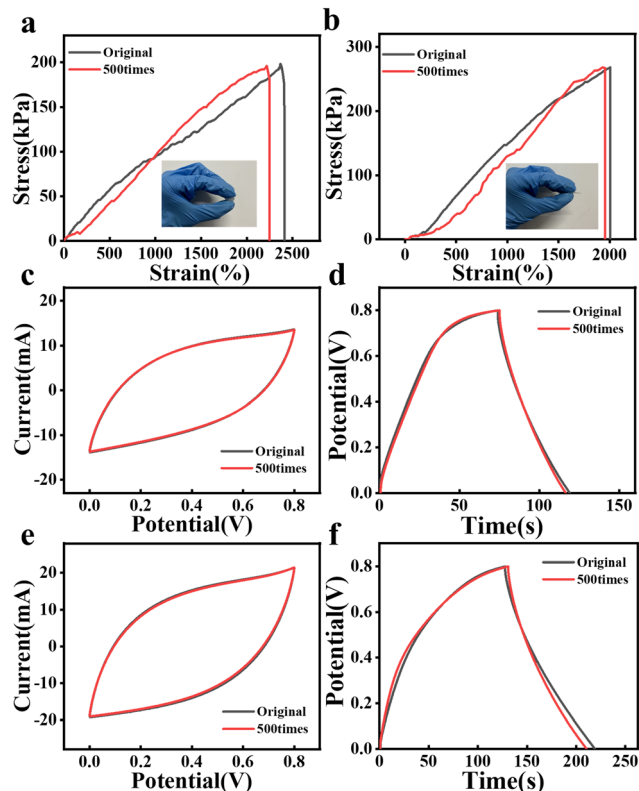
2068 | J. Mater. Chem. C, 2024, **12**, 2063–2072

This journal is © The Royal Society of Chemistry 2024

Fig. 7 (a) Stress−strain curves of the 2P-CE hydrogel before and after 500 cycle numbers bending at 180°. (b) Stress−strain curves of the 2P-CE-L10 hydrogel before and after 500 cycle numbers bending at 180°. (c) and (d) CV curves and GCD curves of the 2P-CE hydrogel before and after 500 cycle numbers bending at 180°. (e) and (f) CV curves and GCD curves of the 2P-CE-L10 hydrogel before and after 500 cycle numbers bending at 180°.
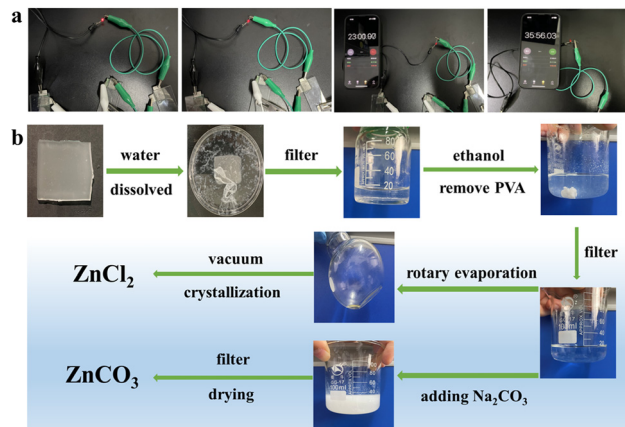

Fig. 8 (a) Pictures of the LED bulb illuminated using the assembled capacitor with the PVA/cellulose hydrogel. (b) Recycling process of Zn salts in the composite hydrogel.

was charged in series with two 1.5 V dry batteries. After 3 minutes, an LED light bulb was connected, and it lit up immediately. With time, the brightness gradually decreased until the bulb extinguished, with the entire illumination process lasting about 33 minutes (Fig. 8a). The experimental results demonstrate that the PVA/cellulose hydrogel electrolyte holds significant actual energy storage and application potential.

Subsequently, the hydrogel after testing was subjected to solvent recovery (Fig. 8b). The PVA/cellulose hydrogel electrolyte was dissolved and dispersed in deionized water. When a large amount of deionized water was added, zinc chloride detached from cellulose and combined with water molecules. Through centrifugation and filtration, a solution of PVA and zinc chloride was obtained. By adding ethanol, PVA could be precipitated. The mixed solution was then rotary evaporated to remove most of the solvent, yielding a concentrated salt solution. Vacuum crystallization could then be used to recover $ZnCl_2$ salt. Adding a solution of sodium carbonate to the mixed solution easily produced $ZnCO_3$. This is commonly used in skin protectants and latex product materials. The target product could be obtained by filtering and drying the white precipitate (Fig. S6a, ESI†). XRD testing of zinc carbonate is shown in Fig. S6b (ESI†), confirming the successful production of relatively pure $ZnCO_3$

solids. The calculated recovery rate is above 55%. This indicates that the application of the PVA-cellulose hydrogel aligns with the principles of green environmental protection, while also possessing certain economic benefits.[45] This opens up new prospects for the application of cellulose-based hydrogel electrolytes.

Experimental

Materials

Polyvinyl alcohol (PVA, DP1750 $\pm$ 50), anhydrous zinc chloride ($ZnCl_2$) (AR 95%), anhydrous calcium chloride ($CaCl_2$) (AR 95%), anhydrous sodium carbonate (Na_2CO_3) (AR 95%), sodium tetraborate $Na_2B_4O_7$ (AR 99.5%), 60 wt% polytetrafluoroethylene (PTFE) aqueous solution, and anhydrous ethanol were sourced from China National Pharmaceutical Group Chemical Reagent Co., Ltd. Cotton short fibers (DP800) were supplied by Xuzhou Lilacan Health Materials Co., Ltd. LiCl (AR 95%) was obtained from Tianjin Fengchuan Chemical Reagent Technology Co., Ltd. Activated carbon and acetylene black were provided by Nanjing Pioneer Nanotechnology Co., Ltd. Nickel foam was supplied by Tianjin Anno New Energy Technology Co., Ltd.

Sample preparation

Preparation of the PVA/cellulose hydrogel electrolyte. PVA solid powder was dissolved in deionized water at 98 °C to obtain a 7 wt% PVA aqueous solution. Zinc chloride was dissolved in deionized water at 65 °C to prepare a 68 wt% zinc chloride solution. Cellulose was then completely dissolved in the zinc chloride solution, resulting in a clear and transparent cellulose solution (1 wt%). The cellulose solution and PVA aqueous solution were mixed in different mass ratios. 0.2 grams of the calcium chloride solid was dissolved in 2 grams of deionized water to prepare a cellulose crosslinking agent solution, which was added to the above mixed solution. Then, 0.3 grams of the boric acid crosslinking agent was introduced to crosslink the PVA. After thorough mixing, the mixture was allowed to stand to

This journal is © The Royal Society of Chemistry 2024

J. Mater. Chem. C, 2024, **12**, 2063–2072 | **2069**

remove bubbles. Subsequently, it was poured into a Petri dish mold while still hot and allowed to cool to solidify at room temperature. This yielded the PVA/cellulose hydrogel electrolyte with a dual crosslinked network (refer to Table S1, ESI†).

Preparation of the 2P-CE-LX hydrogel. The PVA/zinc chloride-cellulose hydrogel (2P-CE) was immersed in an electrolyte solution consisting of 20 wt% $CaCl_2$ and varying LiCl concentrations (refer to Table S2, ESI†). It was allowed to stand for 24 hours until the solution was uniformly absorbed, resulting in the 2P-CE-LX hydrogel electrolyte.

Preparation of symmetric supercapacitors with activated carbon. Commercial activated carbon was used as the active material for the electrodes. Ethanol was used as the solvent. Activated carbon (AC) powder, acetylene black (AB), and polytetrafluoroethylene (PTFE) were mixed in a mass ratio of 8 : 1 : 1 to form a uniform slurry. This mixture was evenly coated onto a foam nickel substrate (1×2 cm) with an area of 1 cm^2. The coated electrodes were dried in a vacuum oven at 80 °C for 12 hours, and then compressed for 25 seconds under a 10 MPa pressure. The assembly of the supercapacitor followed a sandwich structure, with activated carbon/foam nickel electrodes on the top and bottom layers, and the previously prepared PVA/cellulose hydrogel electrolyte as the separator.

Preparation of zinc/activated carbon asymmetric supercapacitors. Zinc sheets were cut into rectangular strips of 1×2 cm, and the zinc oxide layer on the surface was polished off using sandpaper. They were then thoroughly cleaned using anhydrous ethanol and deionized water through repeated ultrasonication, followed by drying in an 80 °C oven to obtain zinc electrodes. The zinc/activated carbon asymmetric supercapacitor was assembled with the PVA/zinc chloride-cellulose hydrogel as the electrolyte, zinc electrodes, and the aforementioned activated carbon electrodes, adopting a sandwich structure.

Characterization and measurements

Mechanical properties. Tensile strength tests were conducted on PVA composite hydrogels with varying cellulose and LiCl contents, as well as on the "integrated" supercapacitors, using an electronic universal testing machine (SANSCMT4503). Prior to testing, the composite hydrogels were molded into dumbbell-shaped specimens, and the testing speed was set at 5 mm min^{-1} (ASTM F2512-20a).

Scanning electron microscopy (SEM). The composite hydrogels were freeze-dried at -80 °C and then gold-sputtered for the observation of the gel fracture surface using a field emission scanning electron microscope (NANOSEM 450).

Fourier transform infrared spectroscopy (FT-IR). The composite hydrogel was completely dried in a freeze dryer at -80 °C, and samples were analyzed by infrared scanning of samples using Fourier infrared spectroscopy (NEXUS, USA) in the wavelength range between 4000 cm^{-1} and 500 cm^{-1} (performed in the ATR mode).

X-ray diffraction (XRD). The dried composite hydrogels were analyzed for the crystal structure and phase composition using X-ray diffraction (XRD, Bruker D8 ADVANCE, Germany). The measurements were conducted under Cu Kα radiation ($\lambda = 1.5418$ Å), with a scanning speed of 5° min^{-1}, collecting X-ray diffraction patterns between 10° and 90° (2θ).

Differential scanning calorimetry (DSC). The composite hydrogel samples were scanned using a NETZSCH DSC200F3 with a heating rate of 10 °C min^{-1} under a N$_2$ atmosphere from 30 to 320 °C.

Electrochemical performance. The assembled supercapacitors were tested using an electrochemical workstation (CHI660e, Shanghai, China). The operating voltage range was set at 0 to 0.4 V or 0 to 0.8 V, and cyclic voltammetry (CV) tests were conducted at different scan rates. Galvanostatic charge–discharge (GCD) tests were performed at different current densities. Electrochemical impedance spectroscopy (EIS) was used to measure the resistance of the supercapacitors within a frequency range of 0.01 Hz to 100 kHz. The formulas for calculating the ionic conductivity (σ in S cm^{-1}), areal specific capacitance (C_s in mF cm^{-2}), energy density (E in mW h cm^{-2}), and power density (P in mW cm^{-2}) of the supercapacitors are as follows:

$$\sigma = L/S_{Res}$$

where L (cm) represents the thickness of the hydrogel electrolyte, S (cm^2) denotes the effective contact area between the electrode and the electrolyte, and Res (Ω) signifies the bulk resistance obtained from the electrochemical impedance spectroscopy (EIS) test.

$$C_s = I\Delta t/S\Delta V$$

where I (mA) represents the designated current density, S (cm^2) stands for the effective contact area between the electrode and the electrolyte, Δt (s) signifies the discharge time, and ΔV (V) indicates the operating voltage range.

$$E = C_s\Delta V^2/7200$$

where C_s (mF cm^{-2}) is the area capacitance of the supercapacitor, and ΔV (V) is the operating voltage range.

$$P = 3600E/\Delta t$$

where E (mW h cm^{-2}) represents the energy density of the supercapacitor, and Δt (s) denotes the discharge time.

Conclusions

Herein, a multifunctional PVA/cellulose composite hydrogel electrolyte was successfully prepared using a simple and environmentally friendly method, demonstrating outstanding performance characteristics including high flexibility, high specific capacitance, excellent low-temperature tolerance, and self-healing properties. Additionally, the recyclability of the hydrogel zinc chloride solvent was investigated. Among the hydrogels studied, the 2P-CE hydrogel exhibited optimal mechanical properties, with a tensile strength and elongation at break reaching 198 kPa and 2413%, respectively. Furthermore, the assembled supercapacitor based on the 2P-CE hydrogel maintained a capacitance retention of 94% at -30 °C. Additionally, the derived 2P-CE-L10 hydrogel electrolyte showcased a high specific capacitance of 636 mF cm^{-2} in a zinc/activated

2070 | *J. Mater. Chem. C*, 2024, **12**, 2063–2072

This journal is © The Royal Society of Chemistry 2024

carbon asymmetric supercapacitor. The assembled supercapacitor was able to sustainably illuminate an LED bulb for 33 minutes after a 3 minute charge. Notably, even after 1 hour of self-healing, the assembled capacitor still retained a capacitance retention rate of over 94%, indicating outstanding self-healing performance. Finally, through a simple solvent recovery process, zinc chloride and zinc carbonate could be easily obtained, with a zinc ion recovery rate exceeding 55%. This achievement facilitates the recycling and application of zinc salts, bearing significant environmental and economic implications in large-scale production. Therefore, these environmentally friendly PVA/cellulose composite hydrogels hold immense potential in the field of flexible supercapacitors.

Conflicts of interest

There are no conflicts to declare.

Acknowledgements

Notes and references

1 D. P. Dubal, N. R. Chodankar, D. H. Kim and P. Gomez-Romero, *Chem. Soc. Rev.*, 2018, **47**, 2065–2129.

2 C. Hou, T. Huang, H. Wang, H. Yu, Q. Zhang and Y. Li, *Sci. Rep.*, 2013, **3**, 3138.

3 Z. Wei, J. H. Yang, J. Zhou, F. Xu, M. Zrinyi, P. H. Dussault, Y. Osada and Y. M. Chen, *Chem. Soc. Rev.*, 2014, **43**, 8114–8131.

4 H. Su, B. Wang, Z. Sun, S. Wang, X. Feng, Z. Mao and X. Sui, *Carbohydr. Polym.*, 2022, **277**, 118878.

5 W. Kong, C. Wang, C. Jia, Y. Kuang, G. Pastel, C. Chen, G. Chen, S. He, H. Huang, J. Zhang, S. Wang and L. Hu, *Adv. Mater.*, 2018, **30**, e1801934.

6 M. Hu, J. Wang, J. Liu, J. Zhang, X. Ma and Y. Huang, *Chem. Commun.*, 2018, **54**, 6200–6203.

7 J. Hu, Y. Wu, Q. Yang, Q. Zhou, L. Hui, Z. Liu, F. Xu and D. Ding, *Carbohydr. Polym.*, 2022, **275**, 118697.

8 Y. Heng, T. Xie, X. Wang, D. Chen, J. Wen, X. Chen, D. Hu, N. Wang and Y. A. Wu, *Nanotechnology*, 2021, **32**, 095403.

9 C. W. Irvin, C. C. Satam, J. Liao, P. S. Russo, V. Breedveld, J. C. Meredith and M. L. Shofner, *Biomacromolecules*, 2021, **22**, 340–352.

10 J. Chen, X. Shi, L. Ren and Y. Wang, *Carbon*, 2017, **111**, 18–27.

11 K. Wang, X. Zhang, C. Li, X. Sun, Q. Meng, Y. Ma and Z. Wei, *Adv. Mater.*, 2015, **27**, 7451–7457.

12 X. Zhu, C. Ji, Q. Meng, H. Mi, Q. Yang, Z. Li, N. Yang and J. Qiu, *Small*, 2022, **18**, e2200055.

13 H. Zhang, H. Xia and Y. Zhao, *ACS Macro Lett.*, 2012, **1**, 1233–1236.

14 X. Rui-Hong, R. Peng-Gang, H. Jian, R. Fang, R. Lian-Zhen and S. Zhen-Feng, *Carbohydr. Polym.*, 2016, **138**, 222–228.

15 T. Xu, D. Yang, S. Zhang, T. Zhao, M. Zhang and Z.-Z. Yu, *Carbon*, 2021, **171**, 201–210.

16 J. Tian, Z. Sun, C. Shi and Z. Huang, *Int. J. Biol. Macromol.*, 2023, **248**, 125937.

17 K.-h Zhu, X.-d Han, S.-f Ye, P.-x Cui, L.-y Dou, W.-b Ma, S. Heng, X.-y Tao and X.-y Wei, *J. Energy Storage*, 2022, **53**, 105096.

18 Y. Liu, W. Wang, K. Gu, J. Yao, Z. Shao and X. Chen, *ACS Appl. Mater. Interfaces*, 2021, **13**, 29008–29020.

19 X. Fan, R. Zhang, S. Sui, X. Liu, J. Liu, C. Shi, N. Zhao, C. Zhong and W. Hu, *Angew. Chem., Int. Ed.*, 2023, **62**, e202302640.

20 J. Yin, K. Wei, J. Zhang, S. Liu, X. Wang, X. Wang, Q. Zhang, Z. Qin and T. Jiao, *Cell Rep. Phys. Sci.*, 2022, **3**, 100893.

21 L. Guo, W.-B. Ma, Y. Wang, X.-Z. Song, J. Ma, X.-D. Han, X.-Y. Tao, L.-T. Guo, H.-L. Fan, Z.-S. Liu, Y.-B. Zhu and X.-Y. Wei, *J. Alloys Compd.*, 2020, **843**, 157686.

22 Z. Zhang, C. Yu, Z. Peng and W. Zhong, *Cellulose*, 2020, **28**, 389–404.

23 D. Meng, C. Wu, Y. Hu, Y. Jing, X. Zhang, S. Mahmud, S. P. Su and J. Zhu, *J. Energy Storage*, 2022, **51**, 104341.

24 J. Liu, X. Meng, F. Dong, S. Ren, B. Wang and F. Tan, *ACS Appl. Polym. Mater.*, 2022, **4**, 8216–8226.

25 J. Yu, Y. Feng, D. Sun, W. Ren, C. Shao and R. Sun, *ACS Appl. Mater. Interfaces*, 2022, **14**, 10886–10897.

26 C. Chen, Y. Wang, Q. Wu, Z. Wan, D. Li and Y. Jin, *Chem. Eng. J.*, 2020, **400**, 125876.

27 G. Yan, S. He, S. Ma, A. Zeng, G. Chen, X. Tang, Y. Sun, F. Xu, X. Zeng and L. Lin, *Chem. Eng. J.*, 2022, **427**, 131896.

28 G. Chen, T. Li, C. Chen, W. Kong, M. Jiao, B. Jiang, Q. Xia, Z. Liang, Y. Liu, S. He and L. Hu, *ACS Nano*, 2021, **15**, 11244–11252.

29 Z. Wang, Z. Zhou, S. Wang, X. Yao, X. Han, W. Cao and J. Pu, *Composites, Part B*, 2022, **239**, 109954.

30 Z. Peng, Y. Zou, S. Xu, W. Zhong and W. Yang, *ACS Appl. Mater. Interfaces*, 2018, **10**, 22190–22200.

31 D. Chen, X. Zhao, X. Wei, J. Zhang, D. Wang, H. Lu and P. Jia, *ACS Appl. Mater. Interfaces*, 2020, **12**, 53247–53256.

32 Q. F. Guan, H. B. Yang, Z. M. Han, Z. C. Ling, C. H. Yin, K. P. Yang, Y. X. Zhao and S. H. Yu, *ACS Nano*, 2021, **15**, 7889–7898.

33 N. Zhao, F. Wu, Y. Xing, W. Qu, N. Chen, Y. Shang, M. Yan, Y. Li, L. Li and R. Chen, *ACS Appl. Mater. Interfaces*, 2019, **11**, 15537–15542.

34 P. Zhang, M. Li, Y. Jing, X. Zhang, S. Su, J. Zhu and N. Yu, *J. Mater. Sci.*, 2023, **58**, 1694–1707.

35 H. Wang, J. Wu, J. Qiu, K. Zhang, J. Shao and L. Yan, *Sustainable Energy Fuels*, 2019, **3**, 3109–3115.

This journal is © The Royal Society of Chemistry 2024

J. Mater. Chem. C, 2024, **12**, 2063–2072 | **2071**

36 L. Alves, B. Medronho, A. Filipe, A. Romano, M. G. Rasteiro, B. Lindman, D. Topgaard, I. Davidovich and Y. Talmon, *Carbohydr. Polym.*, 2021, **252**, 117122.

37 X. F. Zhang, X. Ma, T. Hou, K. Guo, J. Yin, Z. Wang, L. Shu, M. He and J. Yao, *Angew. Chem., Int. Ed.*, 2019, **58**, 7366–7370.

38 G. Chen, F. F. Hong, J. Yuan, L. Li, M. Fang, W. Wei, X. Wang and Y. Wei, *Carbohydr. Polym.*, 2022, **296**, 119917.

39 L. Shu, X. F. Zhang, Z. Wang and J. Yao, *Carbohydr. Polym.*, 2022, **275**, 118695.

40 L. C. Wong, C. P. Leh and C. F. Goh, *Carbohydr. Polym.*, 2021, **264**, 118036.

41 Y. Song, L. Niu, P. Ma, X. Li, J. Feng and Z. Liu, *ACS Appl. Mater. Interfaces*, 2023, **15**, 10006–10017.

42 J. Zhou, M. Xie, F. Wu, Y. Mei, Y. Hao, L. Li and R. Chen, *Adv. Mater.*, 2022, **34**, e2106897.

43 M. A. Saadiah, Y. Nagao and A. S. Samsudin, *Int. J. Hydrogen Energy*, 2020, **45**, 14880–14896.

44 K. Zhang, Y. Pang, C. Chen, M. Wu, Y. Liu, S. Yu, L. Li, Z. Ji and J. Pang, *Carbohydr. Polym.*, 2022, **293**, 119673.

45 Y. Ma, J. Yin, H. Liang, D. Yao, Y. Xia, K. Zuo and Y.-P. Zeng, *J. Cleaner Prod.*, 2021, **279**, 123786.